Mechanical characterization and frequency analysis of a 40 mN.m.s reaction wheel

AUZOUX Jérémie [1], RENARD Mathieu [2], DESCHAUX Flavien [3], PILLOY Baptiste [4]

[1] *6 Chem. de Vignalis, 31130 Flourens, France, +33 5 61 24 26 16, j.auzoux@comat.space*
[2] *6 Chem. de Vignalis, 31130 Flourens, France, +33 5 61 24 79 56, m.renard@comat.space*
[3] *6 Chem. de Vignalis, 31130 Flourens, France, +33 5 61 24 26 16, f.deschaux@comat.space*
[4] *6 Chem. de Vignalis, 31130 Flourens, France, +33 5 61 24 26 16, b.pilloy@comat.space*

1. ASBTRACT

The aim of this publication is to define a reliable, fast and simple method to characterize a 40 mN.m.s reaction wheel, manufactured and assembled by COMAT for nanosatellites market. The idea is to define a set of tests using a six-axis Kistler dynamometer in order to understand the mechanical behavior of the wheel, its health and configuration. Then, comparing the results with performance criteria, COMAT can quickly define if the tested wheel has defects and which part is involved. To have access to this information, COMAT wants to set up a quick and easy method. Two tests were then developed: the first consists in reaching a rotation speed of 6000RPM by steps of 50RPM. It allows to obtain the micro-vibration signature of the wheels and to calculate the static and dynamic unbalances. The second test consists in sending a range of sinusoidal speed command with an increasing frequency to obtain the tracking error and the Bode diagram of the wheel.

2. NOMENCLATURE

c_r, c_a Radial and axial damping factor respectively
d Distances
f Frequency
F Force
φ Phase
G_{db} Gain
h Engine order
i General index
I_z Axial inertia
j Imaginary unit
k_r, k_a Radial and axial bearing stiffness respectively
K Static gain
m Mass
M_d Torque caused by the dynamic unbalance
ω_n Natural frequency or pulsation
Ω Reaction wheel rotor speed
r Ratio of d_2 to d_1
r_s, r_d Radial distance from the rotor Center of Mass to static and dynamic unbalance mass, respectively
T Time period
U_s, U_d Static unbalance and dynamic unbalance respectively

3. INTRODUCTION

Comat designs, manufactures, qualifies and commercializes equipment for space industry since 1977. A few years ago, Comat started the development of reaction wheels for satellites. A satellite should remain pointed in a specific orientation in order to perform different missions. Four reaction wheels are then used to master its attitude. Three would be sufficient, but the fourth is used in case one breaks down. The wheel compensates the external torque applied to the spacecraft. Reaction wheels also increase gyroscopic stiffness on satellites requiring little precision, called "zero degree of freedom satellites". Moreover, after ejection of the launcher's upper stage, the satellite has an uncontrolled attitude with high rotation rate. Reaction wheels are then used to detumble the satellite. Finally, the wheels allow to quickly rotate the satellite when a command is sent, this is called satellite agility. Comat manufactures and assembles wheels from the latest reaction wheel generation, plug-and-play, radiation proof, with a long lifetime, safeguarded electronics and a with very compact design.

This publication presents the means used to understand and characterize the mechanical behavior of the wheel using piezoelectric sensors and its electronical response. The idea is to develop a quick and simple measuring technique that allows the best characterization of the mechanical and electronical configuration of the wheels, their good health and their defects. By repeating the tests several times, improving the scripts and the post-processing codes, two typical tests were selected. They allow to obtain a lot of information on the wheel in a short time. These tests are made on wheels with momentum capacities of 40 mN.m.s. All reaction wheels manufactured and assembled by Comat have a brushless motor with three pairs of poles. The titanium bell is made in two parts and has a mass of 75.9 g. The rotating mass m_r of the wheel is equal to 102.74 g (including flywheel, haft, inner rings, spacers, rotor and lock nut). The total mass of the wheel is 246 g, the axial inertia I_z according to z-axis is equal to 6.371×10^{-5} kg.m² and the outside radius of the wheel is 33.5mm.

This publication is organized as follows. In section 4, materials and methods used to carry out the tests are given. In this section, the data acquisition system, the tests performed with the wheels and how the post-processing was done are presented. The section 5 presents the results of the tests, followed by section 6 with discussions on the results obtained.

4. MATERIAL AND METHOD

4.1 Data acquisition system

A Kistler multicomponent piezoelectric dynamometer, type 9306A, is used to measure forces and torques in the three axes x, y and z with high accuracy. When the sensor detects a deformation, small electrical charges are sent to the Kistler amplifier, which converts voltage into forces. Finally, via an RJ45 connection, the measured forces are sent to the computer.
The test bench is composed of:
- X1 Kistler six-axis dynamometer 9306A
- X2 Kistler amplifier LabAmp 5165A4K (one for collecting force data, the other for torque data)
- X1 Decoupled table on a marble table
- X1 Reaction wheel power supply
- X1 Comat portable computer with a LabVIEW program loaded on it
- X1 USB hub

- Connecting cables

4.2 Tests performed

A set of performance tests has been decided in order to obtain the most reliable results characterizing the wheel's behavior in a quick and simple way. The tests are carried out in the ISO7 cleanroom on the test bench described above. The wheel itself gives us information on its rotation speed and the rotor temperature in real time. The wheel is powered by a generator providing 15V. The Figure 1 presents the test configuration. The wheel is directly fixed on a base linked to the piezoelectric sensor as shown in figure 2.
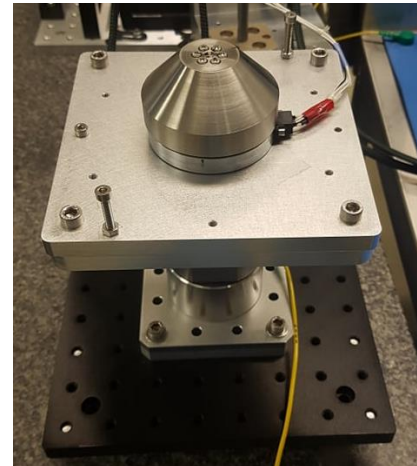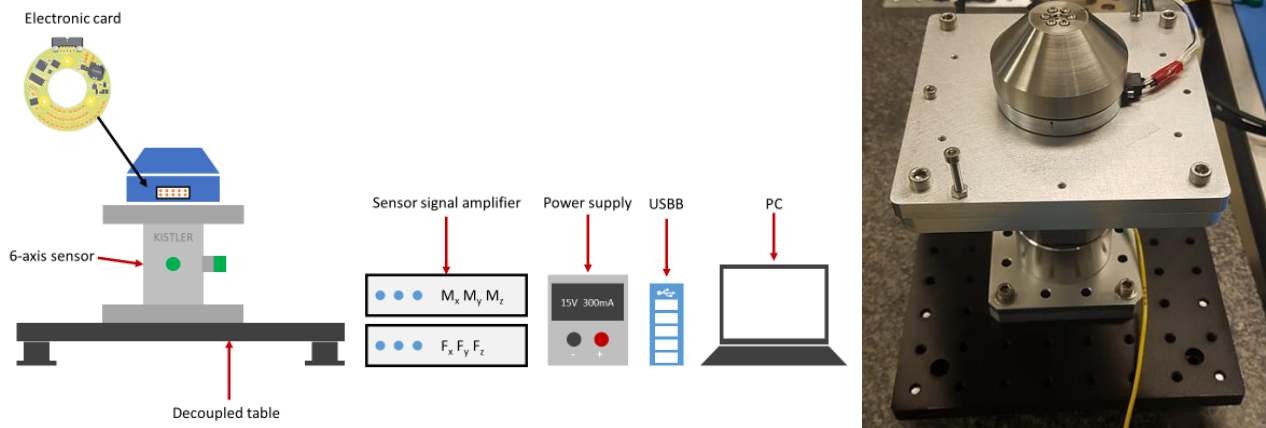
Figures 1 and 2: Test bench configuration

To proceed with the tests, a script is created with MATLAB, then loaded on LabVIEW which sends the instructions directly to the wheel. The LabVIEW code allows to obtain all the information from the wheel and the Kistler sensor in real time. The Human Machine Interface allows to check the ongoing operation. Proportional–integral (PI) corrector parameters can be modified in LabVIEW; these parameters are sent directly to the wheel's on-board servo system.

First test: wheel vibration mapping

With this test, Comat has access to the micro vibration signature of the wheels. It allows to find the natural frequencies of the wheels, to find the impacts of the external environment on the test bench, to calculate the static and dynamic unbalances, and finally to highlight the engine orders, i.e., the manufacturing defects. As [3], a lot of information characterizing the wheel can be obtained with this test.

First of all, we carry out a "tap test" in order to obtain the proper modes of the wheel and the tooling on which it is placed. The Figure 3 shows the method for performing the tap test. The taps are restrained and are made with a soft surface so as not to damage the material. Then, the wheel receives speed instructions in steps: the speed of 6000 Revolutions per minute (RPM) is reached from 400RPM. The speed range is performed with 50RPM speed steps. (Figure 4).
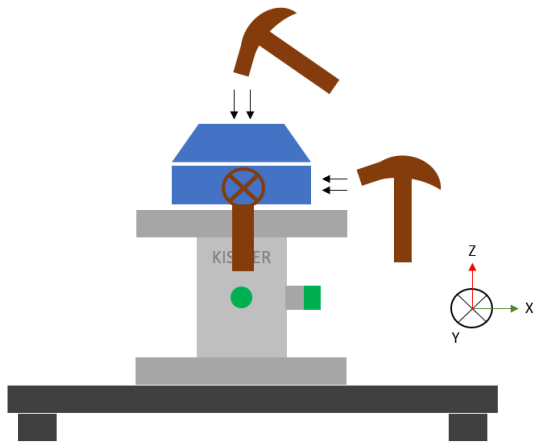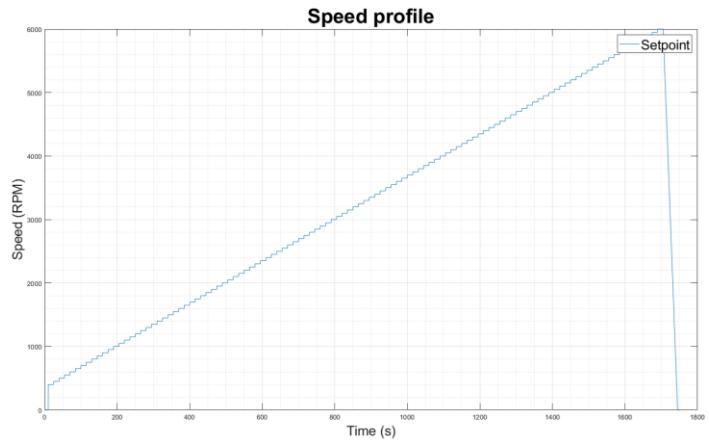
Figure 3 : Tap test configuration

Figure 4: Mapping test speed profile: the wheel reaches 6000RPM in 50RPM steps.

Second test: Bode diagram

We wanted to have access to the tracking error, the cut-off frequency and the phase shift of the wheels. This test was then set up in order to obtain all the information simply. A sinusoidal speed setpoint is sent to the wheel with an increasing frequency. The wheel first reaches a speed of 2000RPM, then the sinusoids have an amplitude of + or - 250RPM (Figure 5).
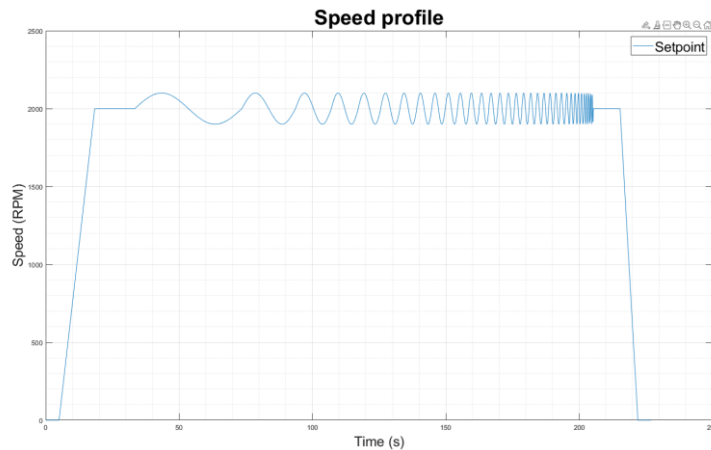

Figure 5: Bode diagram test speed profile

4.3 Data processing

First test: wheel vibration mapping

Once the data is imported, the study areas must be defined as well as the temporal boundaries of these areas. A MATLAB function then calculates the Fast Fourier Transform (FFT) of the vibration forces and torques obtained. First, FFTs are plotted when the wheel is not turning, with the results of the tap test, in order to better understand the impact of the external environment on the tests. Secondly, a waterfall plot is drawn with the frequency from the FFT as the x-axis, the wheel speed as the y-axis and the vibration amplitude (forces and then moments) as the z-axis. The waterfall plot is plotted up from 0 Hz to 2000 Hz, as this is frequency range where the important information lies.

Another code is used to calculate the static unbalance U_s and the dynamic unbalance U_d of the wheel. The static unbalance U_s is caused by a centripetal force F_s and an unbalance mass m_s,

placed at a distance r_s from the axis of inertia, moving about the axis of rotation (Figure 6). This force is equal to the product of this mass m_s, the radius r_s and the rotational speed Ω squared (Equation 1).

$$F_s = m_s \cdot r_s \cdot \Omega^2 = U_s \cdot \Omega^2 \tag{1}$$

where F_s is in Newton, m_s in kg, r_s in meters, U_s in kg.m or g.mm, equal to $m_s * r_s$ and Ω in rad/s.

The dynamic unbalance U_d is due to an inclination of the main axis of inertia relative to the axis of rotation. This inclination can be modelled by two equal masses m_d separated by a distance d_d on the axis of rotation (Figure 7). As the wheel rotates, the centripetal force of each mass causes a torque proportional to the distance d_d (Equation 2).

$$M_d = m_d \cdot r_d \cdot d_d \cdot \Omega^2 = U_d \cdot \Omega^2 \tag{2}$$

where M_d is in N.m, m_d in kg, d_d in meters, U_d in kg.m² or g.mm², equal to $m_d \cdot r_d \cdot d_d$.

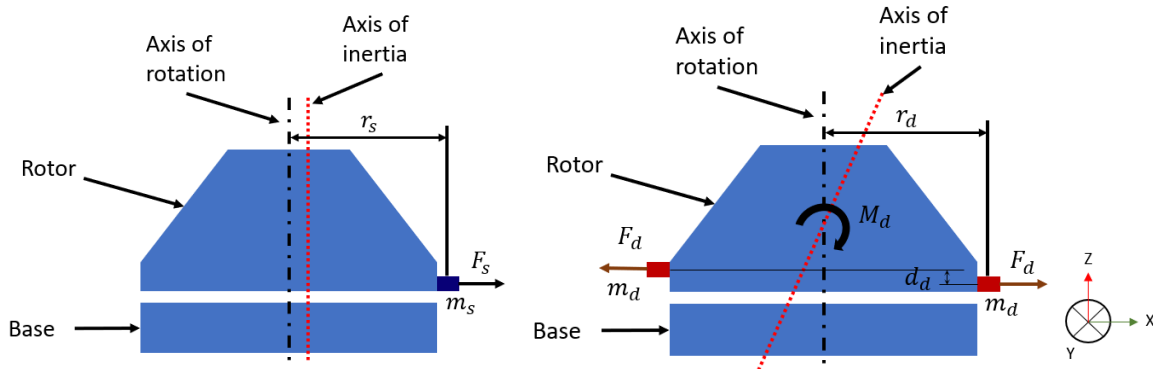Figure 6 and 7: static and dynamic unbalances respectively

The amplitudes of vibrations used to calculate the unbalances are extracted from the F_x, F_y, M_x and M_y waterfall plots when the frequency in Hz, coming from the FFTs, is equal to the speed of rotation of the wheel also in Hz (Equation 3). This is called the fundamental harmonic.

$$\frac{\Omega}{60} = f \tag{3}$$

where f is the frequency given by the FFT in Hz. The extraction of the vibration amplitudes is made at each rotational speed of the wheel in order to have a more reliable unbalance value. Once the unbalance calculations are made at all wheel speed ranges, a statistic Gaussian distribution is used to find the closest value to reality. It is necessary to compare the values recorded between each test and each wheel using the same parameters.

The mapping also allows to highlight the rocking mode (Figure 8). The radial rocking mode corresponds to two whirl modes, a so-called positive whirl mode and a negative whirl mode, which have a natural frequency that depends on the rotation speed of the wheel (Equation 4). The wheel can be modeled according to the form shown in figure 9. Each bearing is represented by a spring and a

dash-pot damper in order to represent the stiffness and the damping of the bearings. The bearings are linked to the rotor on one side and to the ground on the other side.
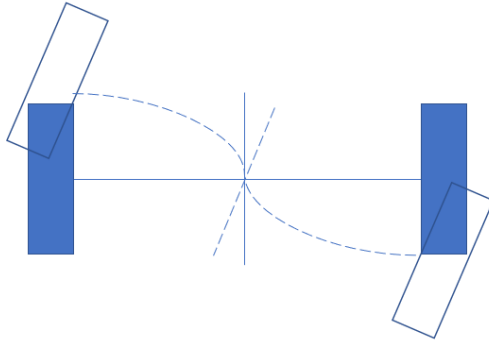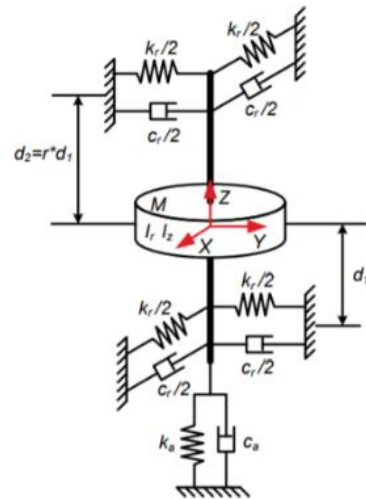

Figure 8: rocking mode   Figure 9: model of the wheel [2]

After a series of calculations [1], two solutions of the differential equation that characterizes the wheel appear, corresponding to two rotational natural frequencies:

$$\omega_{1,2} = \pm \frac{\Omega \cdot I_z}{2 \cdot I_r} + \sqrt{\left(\frac{\Omega \cdot I_z}{2 \cdot I_r}\right)^2 + \frac{k_r \cdot d_2^2}{I_r}} \qquad (4)$$

where $\omega_{1,2}$ is the rotational natural frequency in rad/s, k_r is the bearing radial stiffness in N/m and d_2 is the distance between the upper bearing and the center of gravity of the wheel in meters. These two modes appear as a visual V on the waterfall plots. At zero speed the natural frequency is therefore the same for the positive and negative whirl.

Finally, the engine orders (or harmonic numbers) h are visible on the waterfall plots. They are straight lines starting from the origin and increasing with the rotation speed of the wheel with a slope value *h* (Equation 5). This slope corresponds to the harmonic number. The order one unbalance is called fundamental harmonic because it corresponds to an engine order equal to one (frequency in Hz equal to the speed of rotation also in Hz).

$$h_i = \frac{1}{\left(\Omega/f\right)} \qquad (5)$$

where Ω is the wheel speed and f is the frequency, both expressed in Hz. These engines orders physically correspond to imperfections in the wheel. On the waterfall plots, when an engine order crosses a wheel mode, the vibration amplitude increases sharply because of the sum of both modes. It is important that the rocking mode does not cross the fundamental harmonic so that the vibrations

generated are not too strong. The strong vibrations are important to check as they can have too great impact on the satellite.

Second test: Bode diagram

A MATLAB code is used to draw the Bode diagram of a wheel via the test results. A superimposition of the set speed and response curves is made and then the code looks for the maximum values of the two curves for each frequency. Then the gain is calculated using the Equation 6 and the phase using Equation 7.

$$G_{db} = 20 \cdot \log\left(\frac{\Omega_{r\_max\_i}}{\Omega_{s\_max\_i}}\right) \tag{6}$$

$$\varphi(°) = \frac{\left(t_{s_i} - t_{r_i}\right) \cdot 360}{T_i} \tag{7}$$

where G_{db} is the gain in dB, $\Omega_{r\_\max\_i}$ and $\Omega_{s\_\max\_i}$ are respectively the maximum response and setpoint speed of the wheel at time t_{r_i} and t_{s_i} and at period i, φ is the phase in ° and T_i is the period i in second.

5. RESULTS

All the tests presented above were realized several times with different configurations and on different wheels (40 mN.m.s wheels). The figures presented in this section come from a Comat wheel while the tables presented are the results of several tests on different wheels but with the same mechanical and electronical configuration.

First test: wheel vibration mapping

As a first step, it is interesting to study the frequency responses of the assembly when the wheel is not rotating in order to understand the vibrations that can be generated by the external environment. For this purpose, we carried out a tap test on the KISTLER table. Three configurations were adopted. The first one is with the wheel fixed on the support, in test condition. The second is with a mass having the same physical characteristics as a RW40 (equal mass and inertia). The last one is with the Kistler table alone, without wheel or mass. The results are presented in Table 1 and the analyses of these results are presented in the next section.

Table 2 shows the forces and torques waterfall plots in the X, Y and Z directions from 0 Hz up to 2000 Hz. As for zero speed results, all redundant frequencies with non-negligible amplitudes are listed in a table to discuss their origin. The discussions are presented in the next section. These results come from a Comat Qualification Model (QM). The results are broadly similar for all wheels. Only the vibration levels may change depending on whether the wheel is worn or not.

The calculation of the dynamic and static unbalance was made on three wheels with the same mechanical and electronical characteristics. Table 3 lists the static and dynamic unbalances calculated during the tests on these wheels.
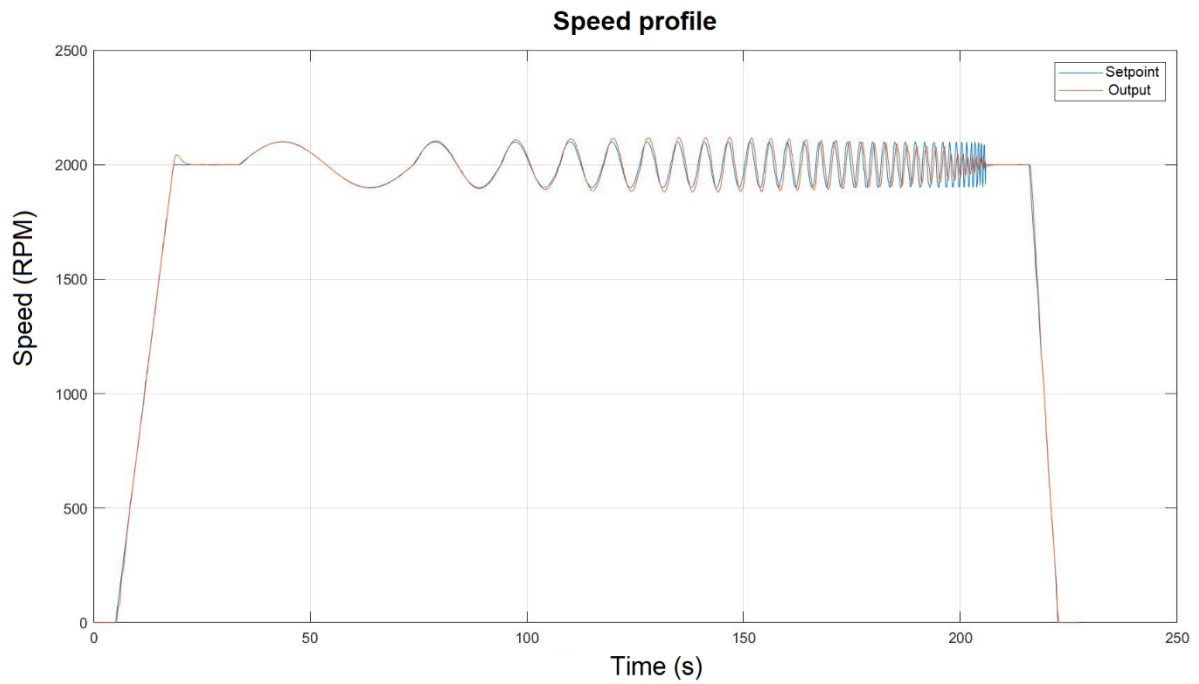
Second test: Bode diagram

Figure 10: superimposition of the speed setpoint and the response. The setpoint is a sinusoid centered on 2000 RPM with an amplitude of + or - 250 RPM.
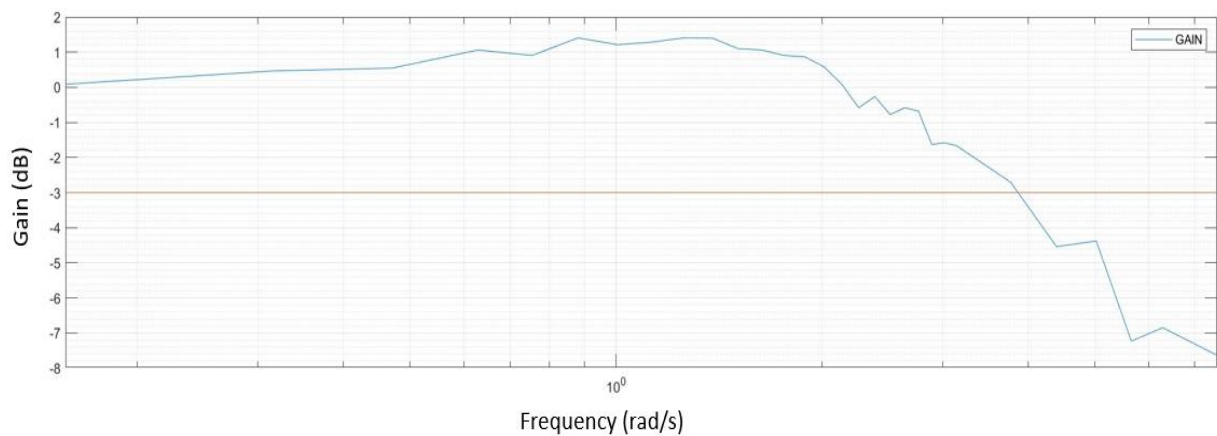

Figure 11: Bode diagram of the wheel

Table 1 : FFT analysis of the tap test in different configurations. The ordinate values are normalized.

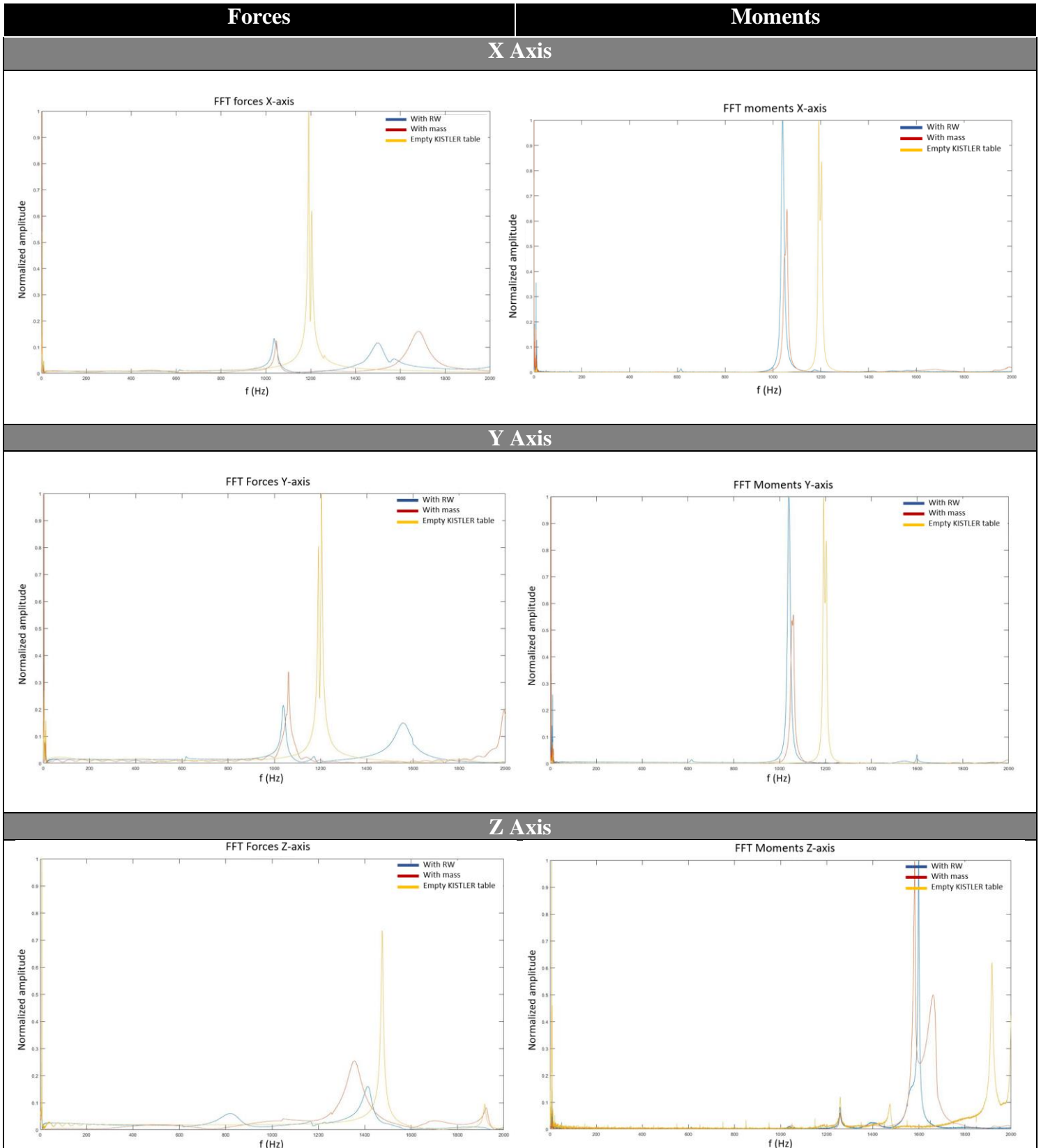| Forces	Moments
X Axis	
Y Axis	
Z Axis	

Table 2 : Waterfall plots. The FFTs calculated at each speed step between 0 and 2000 Hz are aligned to plot these curves in three dimensions. On the left are the force curves and, on the right, the moments curves.
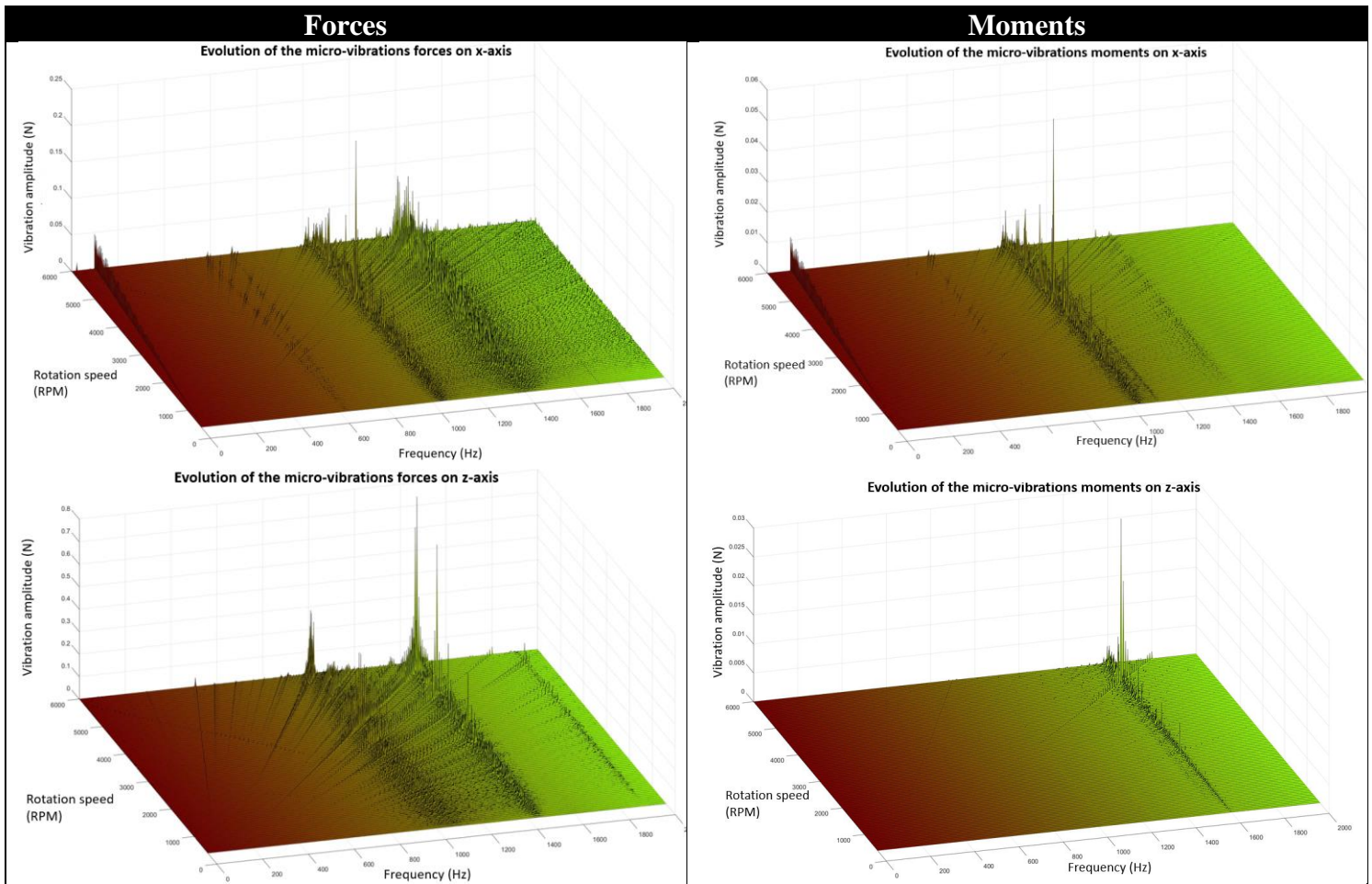

Table 3 : Summary of three reaction wheels unbalances

Wheels	Static unbalance (g.mm)	Dynamic unbalance (g.mm²)
1	0.17	37
2	0.16	42
3	0.13	31

6. DISCUSSIONS

First test: Wheel vibration mapping

On all curves, we notice a little shift between the modes along the x and y axis as well as a difference in the amplitudes. It can be explained by a non-perfect distribution of masses along these two axes during the tests. The sensitivity of the sensor is so high that even the wheel connector accentuates the difference between the X and Y axes. Forces, torques and frequencies of the FFT are not perfectly equal along X and Y axes but the difference is small and can be neglected.

Peaks appear on the curves when the wheel does not turn. In table 1, the peaks visible on the curves are due to the structure placed on the piezoelectric sensor: they are visible on the waterfall plots with a very high amplitude. Moreover, some peaks appear on waterfall plots while they are not

visible on zero speed curves. These peaks correspond to first order unbalance, engine orders or wheel eigenmodes. By repeating the tests with different configurations (without ventilation, changing the axes, etc...), conclusions have been made and are presented in table 4.

It is necessary to check if the modes presented in table 4 do not cross the order 1 unbalance or the rocking mode. The visible lines starting from the origin and evolving with the rotation speed of the wheel are the engine orders due to the imperfections of the wheel. When they cross modes of the wheel, the amplitudes corresponding to the crossing are much higher as we can clearly see in Table 2, on the x axis waterfall plots at 1050 Hz and 4000 RPM. The waterfall plots allow to have a global view on the wheel structure. By looking at these curves, two wheels can be compared. For example, higher amplitudes on engine orders mean that the wheel has defects. Moreover, a shift of the rocking mode means that the parameters of the wheel are different as shown in equations 4.

Table 3 summarizes the static and dynamic unbalances calculated on three wheels. We notice that they all have the same order of magnitude. Environmental vibration and shock tests can vary this value by damaging the wheel. On the other hand, bearing defects can be reduced when the wheel is continuously rotated due to the running-in process, which can decrease the unbalance value. In general, environmental testing has more impact than running-in.
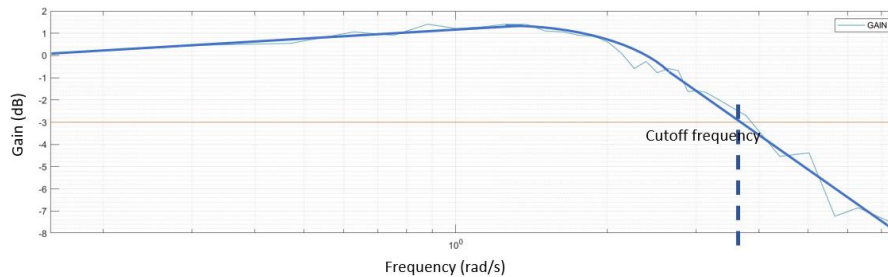
Second test: Bode diagram

Figure 12: Bode diagram of the wheel

When the frequencies are low, the wheel has no trouble following the setpoint. At high frequencies, the wheel follows the setpoint but with a loss of amplitude and a phase shift: this corresponds to the cut-off frequency and the phase drop on the Bode diagram. The cut-off pulsation that appears is about ω_0=3.60 rad/s, i.e a frequency equal to f_c=0.57 Hz or 1.74 seconds. The gain K is equal to 0.1dB, i.e., equal to 1.012 The system is considered as a 1st order system because the inductance is negligible towards the electrical capacity and resistance.
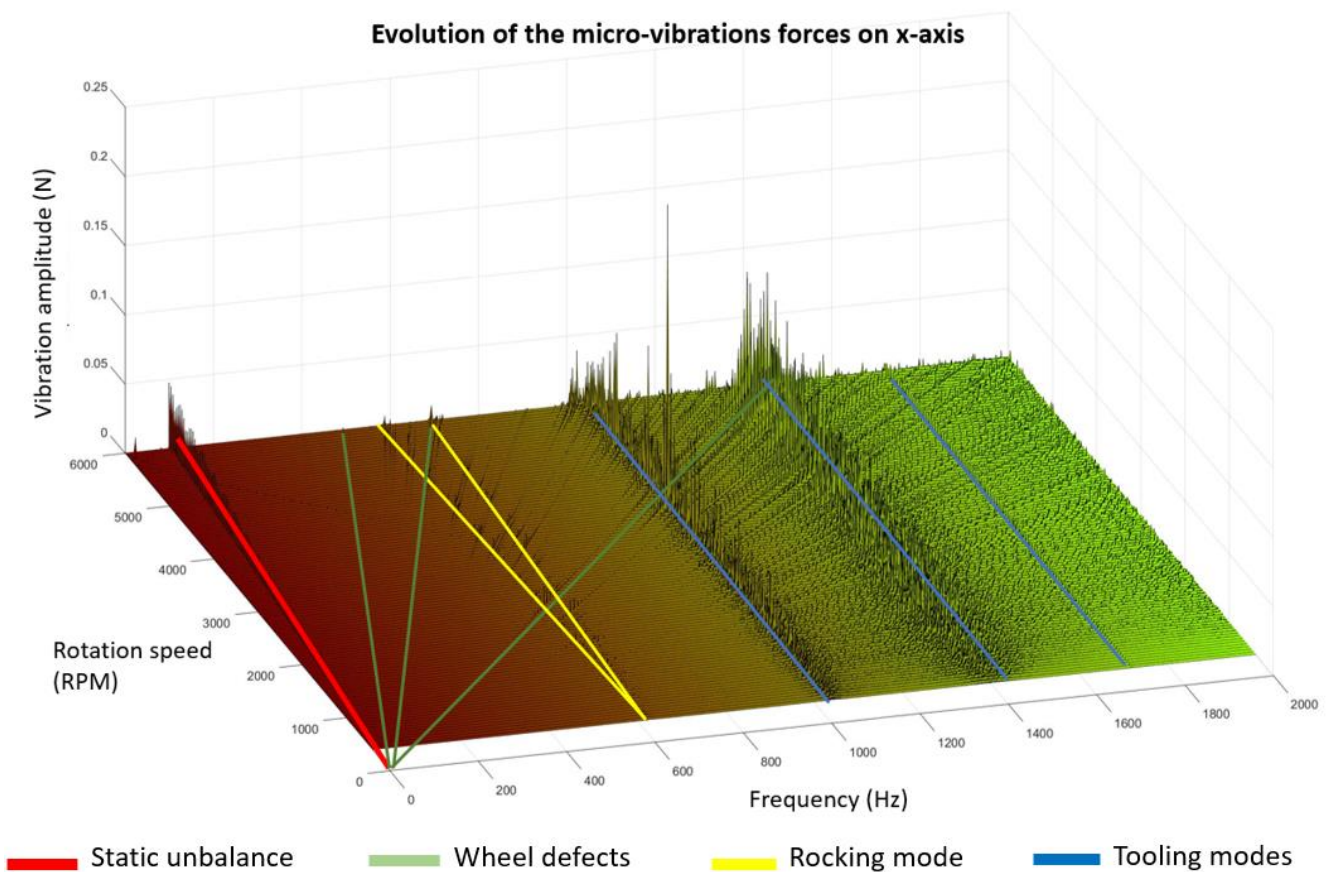
The equation 8 represents the transfer function of the system.

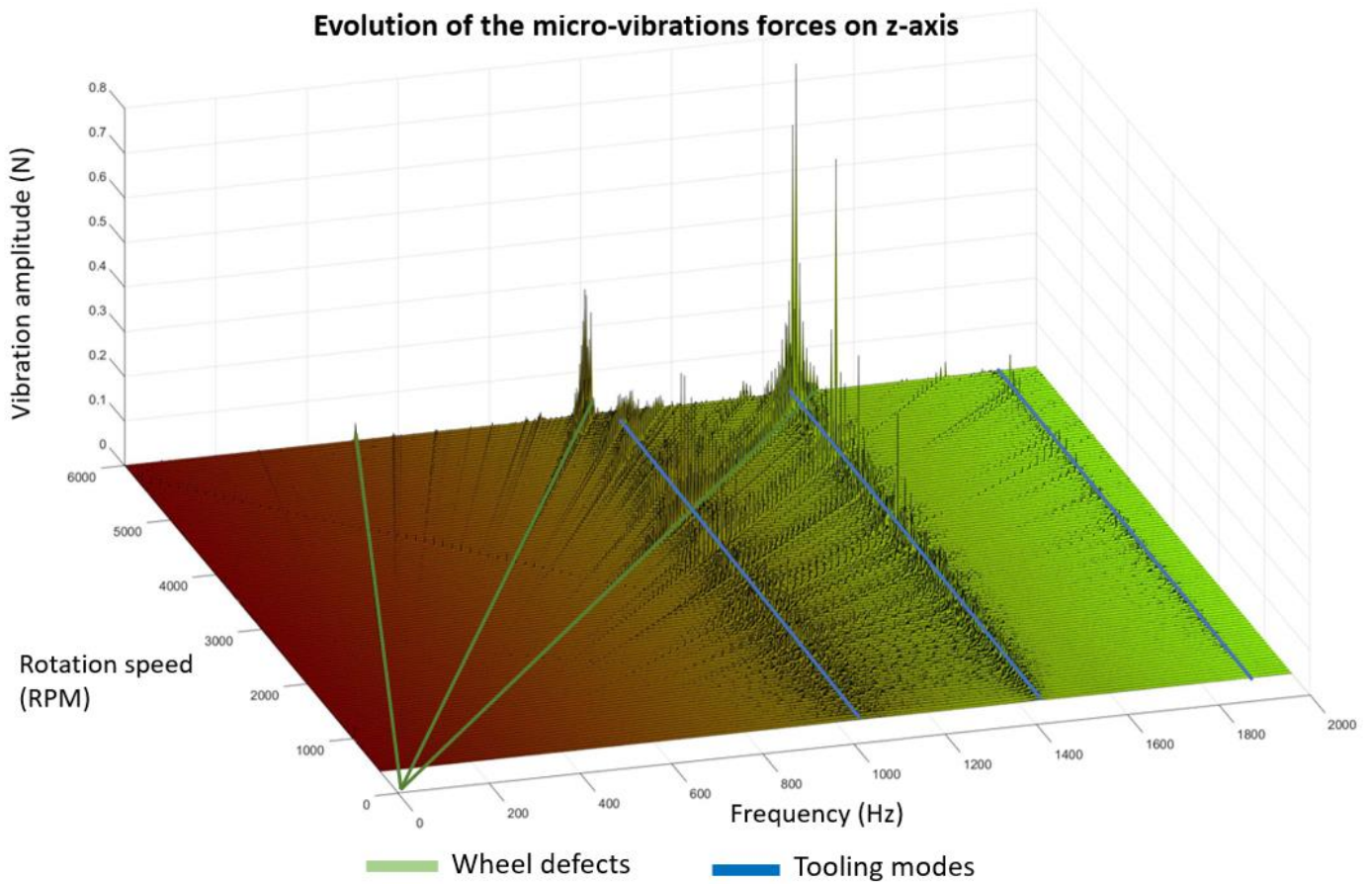$$H(s) = \frac{K}{1 + j\frac{\omega}{\omega_0}} = \frac{1.012}{1 + j\frac{\omega}{3.60}} \tag{8}$$

where ω_0 is the cut-off pulsation, ω is the pulsation, K is the static gain and j is the complex variable.

Table 4 : Summary of all redundant frequencies identified.

Redundant frequencies with high amplitudes x and y axes	Physical correspondence
600 Hz	Rocking mode (V shape on the waterfall plots), not visible when the wheel does not turn
1050 Hz	Tooling mode (wheel + KISTLER table), appears at 1200 Hz when the KISTLER table is empty
1400 Hz	Tooling mode (wheel + KISTLER table)
Redundant frequencies with high amplitudes z-axis	Physical correspondence
1150 Hz	Tooling mode (wheel + KISTLER table)
1400 Hz	Tooling mode (wheel + KISTLER table), appears at 1500 Hz when the KISTLER table is empty
1900 Hz	Tooling mode (wheel + KISTLER table)

Evolution of the micro-vibrations forces on z-axis

Wheel defects — Tooling modes

Evolution of the micro-vibrations moments on x-axis

Static unbalance — Wheel defects — Rocking mode — Tooling modes

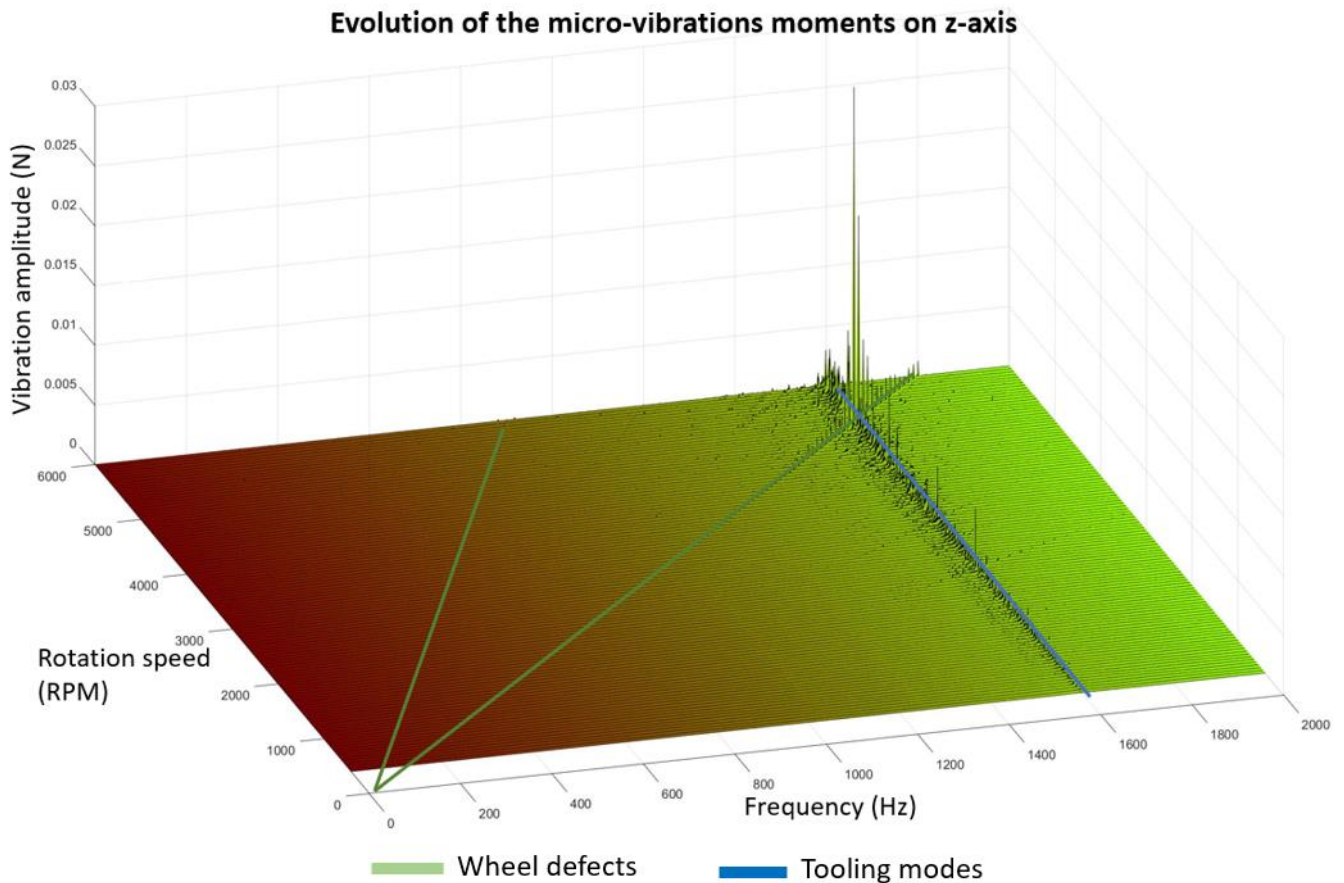**Evolution of the micro-vibrations moments on z-axis**
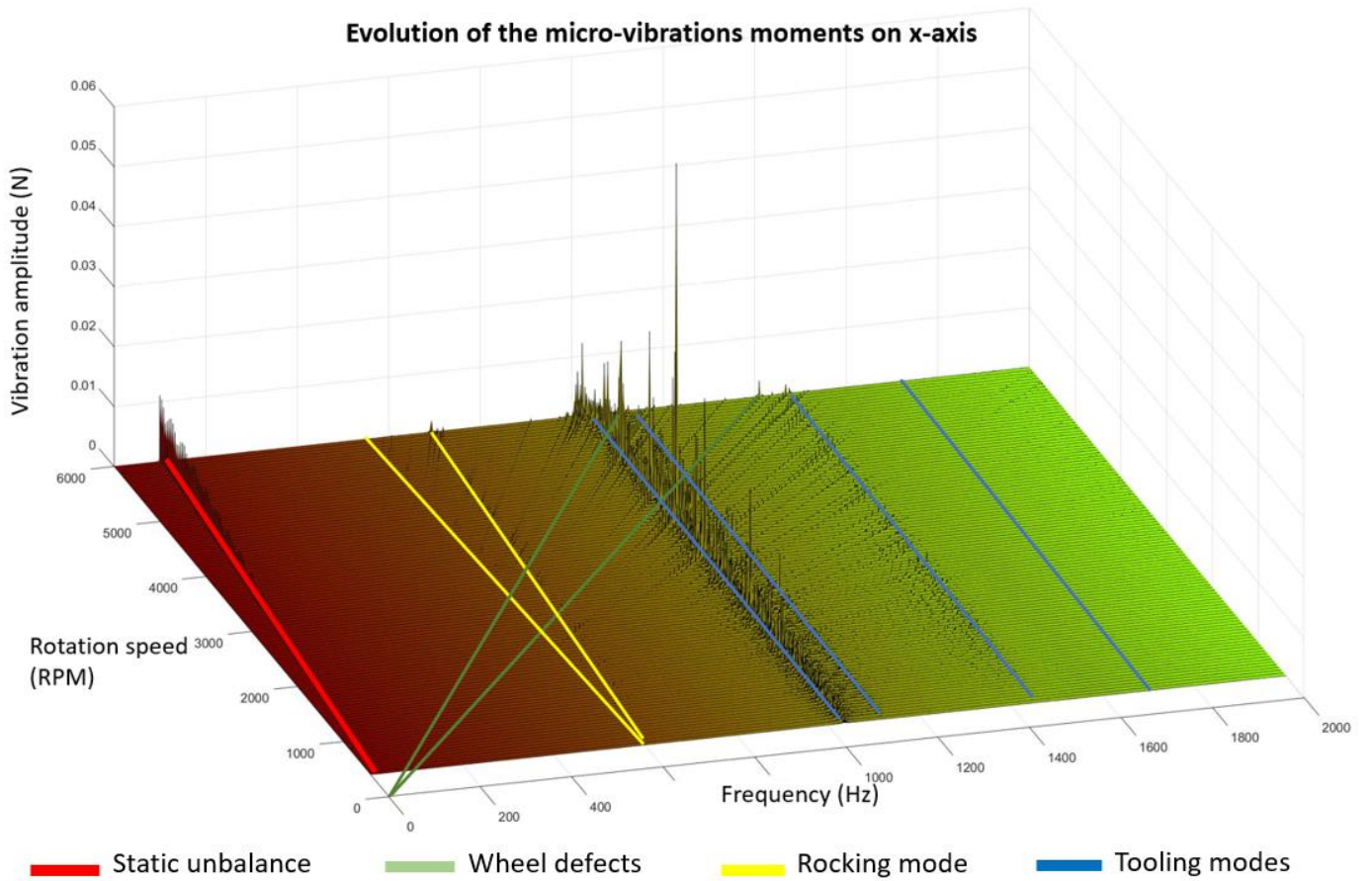
Figure 13, 14, 15 and 16: apparent frequencies on the waterfall plots on the x-axis, in both test configurations

7. CONCLUSIONS

This publication summarizes a study undertaken during several months within Comat. Starting from the idea of obtaining a good mechanical and electronic characterization of reaction wheels (manufactured and assembled by Comat), simple, fast and efficient tests have been set up. Wheel tracking tests and vibration analysis using a KISTLER piezoelectric sensor were carried out in an ISO7 cleanroom. The best results are extracted with an efficient optimization tool, they allow to diagnose the wheel in order to check reliably, quickly and simply its good mechanical health and electronic response. First, a reflection on the frequencies of the FFT, appearing when the wheel is not turning, helped to understand the impact of the external environment on the tests. With the waterfall plots and the unbalance calculation obtained from the wheel vibration mapping test, Comat can find out if the tested wheels have a good mechanical configuration. A shift in the wheel's eigenfrequencies (e.g., rocking mode) which appears on the plots between two tests is evidence of a defect of the wheel or a defect in one of the components. Moreover, an unbalance exceeding the performance criteria defined by Comat means that the unbalance mass is higher and therefore the mechanical configuration of the wheel is not as expected. Finally, the Bode diagram of the wheel has been drawn. It receives a sinusoidal speed setpoint with a lower and lower period in order to obtain the cut-off frequency and the phase shift of the wheel. This allows to quickly determine the correct electronic response of the wheel and its limits.

8. REFERENCES

[1] R. A. Masterson, *Development and Validation of Empirical and Analytical*, Master thesis, MIT, June 1999.

[2] Le, M. P. *Micro-disturbances in reaction wheels*, Eindhoven: Technische Universiteit Eindhoven, 2017.

[3] Shields, Joel, et al. "*Characterization of CubeSat reaction wheel assemblies*." Journal of Small Satellites 6.1 (2017): 565-580.